A model of partial differential equations for HIV propagation in lymph nodes

E. B. S. Marinho[1], F. S. Bacelar[1,2], and R. F. S. Andrade[1]
[1] *Instituto de Física, Universidade Federal da Bahia, 40210-340 Salvador, Bahia, Brazil. and*
[2] *IFISC(CSIC-UIB) Instituto de Física Interdisicplinar y Sistemas Complejos, Campus Universitat Illes Balears, E-07122 Palma de Mallorca, Spain*

(Dated: July 20, 2011)

A system of partial differential equations is used to model the dissemination of the Human Immunodeficiency Virus (HIV) in $CD4^+$T cells within lymph nodes. Besides diffusion terms, the model also includes a time-delay dependence to describe the time lag required by the immunologic system to provide defenses to new virus strains. The resulting dynamics strongly depends on the properties of the invariant sets of the model, consisting of three fixed points related to the time independent and spatial homogeneous tissue configurations in healthy and infected states. A region in the parameter space is considered, for which the time dependence of the space averaged model variables follows the clinical pattern reported for infected patients: a short scale primary infection, followed by a long latency period of almost complete recovery and third phase characterized by damped oscillations around a value with large HIV counting. Depending on the value of the diffusion coefficient, the latency time increases with respect to that one obtained for the space homogeneous version of the model. It is found that same initial conditions lead to quite different spatial patterns, which depend strongly on the latency interval.

PACS numbers: 02.30.Ks,02.30.Hq,87.18.Hf,87.19.Xx

I. INTRODUCTION

The use of dynamical models to describe the infection caused by the the human immunodeficiency virus (HIV) started shortly after its identification as the responsible agent of acquired immunodeficiency syndrome (AIDS) [1–3]. Such studies aimed to describe the time evolution of two blood stream agent populations involved in the infectious process: the HIV and $CD4^+T$ cells, which belong to the immune system (IS) and constitute the main virus target in the human organism [4–7]. The description of the HIV infection by this set of basic variables still dominates. The largest part of the investigated modelswhich take into account the influence of anti-viral drugs [8–11], multiple virus strains [8–13] and more sophisticated description of IS actions have never abandoned these point of view [14, 15].

A quite different approach to describe the HIV dynamics considers what happens to the $CD4^+T$ cells when they are not yet in the blood stream. General lymphocytes are initially produced in the bone marrow, while a fraction of such population is differentiated into $CD4^+T$ in the thyme. There, they may get in contact with HIV and become infected [16]. This is why the fractions of healthy and infected $CD4^+T$ cells in the lymph nodes have been regarded as basic model variables in such alternative framework. Such alternative description of the HIV infection dynamics required the identification of an interaction mechanisms between the healthy and infected cells in the lymph nodes, what was firstly achieved in a cellular automaton (CA) model [17]. Later on, this mechanism was used both within some variants of the CA model [18] and in a model of ordinary differential equations (ODE) with a time delay term [19]. It is important to call the attention that, since this infectious path is based on the assumption of virus spreading in a tissue, it does not include a variable to explicitly describe the virus load on the blood stream.

The purpose of this work is to further explore the alternative interaction mechanism, extending the quoted ODE model to a set of partial differential equations (PDE) to describe the spatiotemporal dynamics of $CD4^+T$ cells on lymph nodes. The used approach considers the following steps to describe the interactions among $CD4^+T$ cells: i) infected cells infect neighboring healthy cells, as in usual contact process; ii) there exists a finite non-zero time lag τ between the moment when one cell is infected and when it dies. During this lag, the attacked cell changes its infecting properties and the IS sets up specific responses to virus strains; iii) new cells produced in the bone marrow replace the dead ones. Usual rate equations can be set up to describe the individual steps of the contact processes and subsequent diffusion. On the other hand, the intrinsic modifications occurring inside the infected cells require the introduction of a time-delay delay term in some of the differential equations.

The system we consider in this work is of a very complex nature, as it combines spacial dependence with effects of time delay. Extending an ODE system to take into account each one of such generalizations amounts to increase the level of mathematical difficulty to identify the solutions of the system of equations or even to characterize their main general properties. From the perspective of numerical integration, a large number ($\to \infty$) of ODE's becomes necessary when we discretize either the space dependence or the time interval associated with the dependence on the solution at past time intervals. Therefore, we were forced to develop and adapt numer-

ical methods to proceed with the numerical integration of the equations of motion.

In spite of such difficulties, we still may count on some basic properties, such that the time-delayed PDE system admits space homogeneous and time independent solutions, which coincide with the fixed-point (FP) solutions of the ODE system [5, 20–22]. As in that case, the set of three FP's greatly influence the time evolution of both homogeneous and inhomogeneous solutions to the PDE system.

This work is organized as follows: In Sec. II, we briefly describe the most important clinical aspects of the HIV infection and derive a suitable PDE model. The meaning of each term in the PDE system and some possible choices of spatial dependence are also discussed. Section III is dedicated to a thorough discussion of the solutions obtained by a numerical integration of our model. Whenever pertinent, properties of ODE fixed points are taken into account to explain and interpret temporal behavior and spatial patterns that emerge in the integration process. Finally, Section IV closes the work with an overview of most relevant ideas brought in this work and perspectives for future investigations.

II. $CD4^+T$ DYNAMICS IN THE LYMPH NODES

The clinical description of non treated HIV infection identifies a fairly constant pattern consisting of three well characterized phases [23]: primary infection, clinical latency and AIDS. The first phase looks much like a typical viremia: it is characterized by a first large increase of HIV in the organism and a subsequent pronounced decline of the virus population, which results from a HIV-specific response set up by the IS. The second phase is asymptomatic and may present large variations depending on the patient health conditions. It is characterized by a very low but persistent HIV counting, indicating that the virus never becomes inactive. The HIV molecular structure changes rapidly, so that new produced strains are always attacking the organism, requiring the IS to produce new specific responses to each of them. Depending on the patient's IS ability, the latency phase may last from a few months to several years. If untreated, the HIV infection may evolve to the AIDS phase, when most patients die by opportunistic infections. This phase is reached when the patient underscores a critical threshold in the $CD4^+T$ cell counting, typically $20 \sim 35\%$ of that of a healthy individual [24].

To describe the $CD4^+T$ infection in the lymph nodes, distinct cell concentrations in a two-dimensional patch of tissue around a point $\overrightarrow{r} = x\widehat{x} + y\widehat{y}$ are selected as the PDE variables. Here x and y indicate the cartesian coordinates of a point while $\widehat{x}$ and $\widehat{y}$ denote the unit vectors along the respective directions. We further assume that the tissue where the cells are located consists of a square domain of area L^2, so that $(x, y) \in ([0, L], [0, L])$. We assume that each such tissue patch is small enough to be considered as a macroscopic infinitesimal and large enough to allow for a continuous concentration variation, as one usually assumes in studies on space dependent biological models [25, 26]. It is further assumed that the target cells can be found in healthy, infected and dead states. Healthy and infected cells are split into two subcategories. We define $H_1(\overrightarrow{r}, t)$ ($H_2(\overrightarrow{r}, t)$) as the concentration of healthy cells that were already born (not yet born) by the time the individual became infected. On the other hand, two types of infected cells are denoted by $A(\overrightarrow{r}, t)$ and $B(\overrightarrow{r}, t)$. The first one describes the amount of newly infected $CD4^+T$, while $B(\overrightarrow{r}, t)$ describes the same infected cells after a given time interval, when they are about to be killed by the action of IS. Finally, $D(\overrightarrow{r}, t)$ describes the concentration of dead cells in the lymph nodes. Since dead cells are also accounted for, the local sum of all variables remains constant over time and is normalized to 1.

The interactions among the quoted variables consider the following basic steps: 1) Healthy cells become infected if they get in contact with infected cells. However, due to the fact that IS provides specific defense to existing virus, cell types H_1 and H_2 require contact with different number of A cells to become infected. 2) Infected A cells change into B cells after some time delay. At such latter stages, B cells have been under attack by IS, so that they are less effective in infecting both H_1 and H_2 healthy cells. 3) B cells die and are replaced by new cells, which can be both in the H_2 or the A states. 4) Larger local concentrations of A cells are subject to a diffusion process to the neighboring tissue patches.

The quoted rules can be translated into the following PDE system:

$$\begin{aligned}
\frac{\partial H_1}{\partial t} &= -k_5 H_1 A^p - k_6 H_1 B^n + k_9 H_1 \nabla^2 A, \\
\frac{\partial H_2}{\partial t} &= k_3 D - k_5 H_2 A^q - k_6 H_2 B^n + k_9 H_2 \nabla^2 A, \\
\frac{\partial A}{\partial t} &= -k_1 A(t-\tau) + k_4 D + k_5 (H_1 A^p + H_2 A^q) \\
&\quad + k_6 (H_1 + H_2) B^n - k_9 (H_1 + H_2) \nabla^2 A, \\
\frac{\partial B}{\partial t} &= k_1 A(t-\tau) - k_2 B, \\
\frac{\partial D}{\partial t} &= -k_3 D - k_4 D + k_2 B. \qquad (1)
\end{aligned}$$

In the above equations, all variables (H_1, H_2, A, B, D) depend on time t and space $\overrightarrow{r}$. For the sake of a simpler notation, we omit this explicit indication, with the exception of the terms that are subject to a delayed time dependence, namely $A(t-\tau)$ that appear in the equations for A and B. The exponent n indicates the order of the contact process between one H and B cells in order that the former become infected-A cells. n assumes the same value for both H_1 and H_2. p and q play similar roles with respect to the contact between A cells with H_1 and

H_2, respectively. Infection of H_1 by A cells is described by a first order process ($p = 1$) but, to express the fact that infection of new born H_2 cells is only slightly less effective than when HIV was first inoculated, the order of infection of H_2 by A cells is assumed to be described by $q \sim 1.1 - 1.2$. Note that, if we set $q = 1$, the equations for H_1 and H_2 become essentially the same, i.e., if we add both equations we obtain a system of four equations for $H = H_1 + H_2, A, B$, and D. This assumption does not produce any qualitative change the solutions of the system, although the very long latency phase obtained when $q \sim 1.1 - 1.2$ becomes reduced reduced. Finally, the contact process of the infection by B cells is assumed to be of much higher order ($n = 4$) [17]. This accounts for the fact already indicated in item (2), that when the cells are about to die, they become much less efficient in transmitting the disease.

The time delay τ required for the IS to mount an specific response is of the order of a few weeks. Therefore, expressing the values of all rate constants in time unit of $week^{-1}$, we consider $\tau = 4$, which is consistent to the clinical observations [27–29] . The time delay term changes, in a crucial way, the dynamics on the phase space, generating trajectories that depend on memory effects. As was discussed in a previous work [19], the presence of non-zero τ may increase the time interval during which the trajectory flows through the slow dynamic region close to two FP's representing healthy states, what allows for the description of the very long latency phase.

Parameters k_1 and k_2 describe the transitions from states A to B and from B to D. The values of two constants that control the interstate transition rate from D to H_2 or A cells can be directly related to two repopulation parameters in the CA model: $k_3 \sim p_{repl}$, the CA rate at which new A-cells are produced. $k_4 \sim p_{repl} * p_{infec} \sim 10^{-5}$ takes into account the value of p_{infec}, the birth probability of infected cells. Finally, the rate constants k_5 and k_6 describe the transition from states H_1 and H_2 to A, in the contact processes discussed previously. The allowed values of k_i are such that 4 constraints must be satisfied: $k_2 > k_1$, $k_5 > k_1$, $k_3 + k_4 > k_2$, $k_3 > k_4$. With such requirements, all the FP coordinates belong to the $[0, 1]$ interval. They also warrant that the following expected relations are satisfied: $A > B > 0$, $D < B$, $p_{repl} > p_{inf}$.

The parameter k_9 denotes the diffusion coefficient of A species, which is responsible for coupling the dynamical evolution between different patches of the lymph node [25, 26]. Two distinct interaction mechanisms can be devised. Diffusion occurs either because infected A cells can move, or because the HIV population, highly concentrated on such cells, can flow together with intersticial liquid and reach new environments, placed at larger distances than the immediate cell neighborhood described by a tissue patch. Since the first mechanism would require the presence of diffusion terms to describe the motion of other cell populations and the corresponding diffusion coefficient would be much smaller, we adopt the second explanation as it is much more realistic. A second relevant issue regarding the diffusion effect of A cells is related to the choice to adopt a non linear mechanism indicated in Eq.(1). A simpler linear description, in which $\nabla^2 A$ is not multiplied either by H_1 or H_2 could, in principle, also be used. However we think the non-linear term is more realistic, as it requires that the diffusive spreading of infection to new cells occurs only in the presence of H_1 or H_2 healthy cells. On the other hand, the simpler linear assumption leads to non physical situations, predicting that infected A cells continue to replace patches where the population of H_1 and H_2 cells have already vanished. This can only occur if they replace B and D cells, what is not a valid step in our model. We also call the attention that diffusion effects do not include cells B. Indeed, these cells are in the last stage of infection and the infection proceeds by a 4-th order contact process. Since it is much less efficient in the infection propagation than that provided by A cells, we decided to make a simpler model by avoiding including a highly non-linear diffusion-like term.

III. RESULTS

a. Choice of parameter values In the previous section we discussed the meaning of all 11 parameters in (1). The actual values of $k_4 = 10^{-5} week^{-1}$, $p = 1$, $n = 4$ and $\tau = 4 week$ were directly obtained from the CA model [17]. We also indicated that, in order to describe clinical observations, the values of several parameters must obey some bounds. They reduce the region in parameter space where useful parameter set should be searched for. Reference [19] reports a number of different time evolution patterns that can be found for the much simpler ODE system. In particular, it has been reported the existence of a region in the parameter space such that the corresponding solutions show the three distinct phases and different time scales of the HIV infection. Herein we take profit of this information and select specific parameter values within the same same region that also lead to such pattern. When non zero values of k_9 are considered and non uniform initial conditions are selected, we obtain many distinct spatial patterns that will presented latter in this section. The choice we make, however, is somewhat distinct from that used in [19], although it also satisfy the same bounds stated before.

b. Homogeneous, time independent solutions To better discuss the space-temporal solutions of system (1), in particular their slow and fast time evolution phases, it is important to understand the properties of its homogeneous, time independent solutions. Homogeneous solutions result when we use uniform initial conditions. In such case, independently of the value of k_9, the solutions do not depend on $\overrightarrow{r}$. In fact, they coincide with those of an ordinary differential equation (ODE) system, which is obtained if we set $k_9 = 0$ in (1). The FP solutions of the corresponding ODE are obtained by setting

all time derivatives to zero. A thorough analysis of the FP's properties has been presented in a previous work [19], so that we will limit ourselves to enumerate their main features.

System (1) has three FP solutions with clear meanings: two of them, $FP_0 = (1, 0, 0, 0, 0)$ and $\widehat{FP_0} = (0, 1, 0, 0, 0)$, obviously describe the states where all $CD4^+T$ cells are healthy. The third one, $FP_1 = (0, \overline{h_2}, \overline{A}, \overline{B}, \overline{d})$, is associated to a steady state in which the organism keeps a fixed proportion of infected $CD4^+T$.

The linear stability analysis easily shows that the healthy states FP_0 and $\widehat{FP_0}$ are unstable both for $\tau = 0$ and $\tau > 0$. FP_0 can only be reached if the initial condition is h_1=1. $\widehat{FP_0}$ has at least one repelling manifold associated with a positive real eigenvalue of the Jacobian matrix $M(\lambda)$=$det(J - \lambda I)$=0, but it can be reached following trajectories that converge to it along the direction of its attractive eigenvectors.

The steady stated described by FP_1 is stable for any value of τ, but this parameter strongly influences the dynamics of the trajectory in its neighborhood. We find that the trajectory decays to FP_1 at a slower rate if $\tau > 0$.

The dependence of the attracting properties of FP_1 on q and τ is such that, when they increase, the dynamics in the phase space region close to FP_1 slows down. For instance, when $\tau > 0$, the real part of the attracting eigenvalues to FP_1 may be reduced by a factor ~ 10 in comparison to its value when $\tau = 0$. Even so, the increase in the time-scale of the latency phase is much larger than such factor. This effect can be accurately described by the flow of the system through regions of very slow dynamics, which can be found in the attracting manifold of $\widehat{FP_0}$. The flow through such region is also controlled by the time-delay terms in (1).

c. Spatiotemporal evolution The system (1) was numerically integrated using a finite difference method, where the time dependence has been treated by a fourth-order Runge-Kutta code adapted to include time-delay effects and the Laplacian operator is approximated by a first order scheme. For this purpose, the effective diffusion coefficient used in the numerical integration is given by $\overline{k_9} = k_9(\delta t/(\delta x)^2)$, where δt and δx set the finite time and length scales. We fixed the value $\delta t = 1/200\ week$ and performed the integration of system (1) for a fixed square sample of unit area $L^2 = 1$ but different grid sizes δx. This way, changes in δx induce a correction in the value of $\overline{k_9}$ in order to hold k_9 fixed. The adopted initial conditions $(H_{1,0}(\overrightarrow{r}), H_{2,0}(\overrightarrow{r}), A_0(\overrightarrow{r}), B_0(\overrightarrow{r}), D_0(\overrightarrow{r}))$ intend to reproduce the typical start phase of the infection, with a small viral load on $CD4^+T$ cells. Therefore, we set $H_{2,0}(\overrightarrow{r}) = B_0(\overrightarrow{r}) = D_0(\overrightarrow{r}) = 0$, $\langle A_0 \rangle \in [0.01, 0.10]$ and $\langle H_{1,0} \rangle \in [0.9, 0.99]$. We adopt periodic boundary conditions throughout this work.

As already mentioned, the choice of uniform initial conditions results in that the thyme tissue follows a time evolution with no spatial modulation, which is equivalent to that one obtained by the ODE model [19]. For non-uniform initial conditions the Laplacian operator induces the formation and evolution of spatial patterns. The importance of the time delay terms is confirmed by its influence in the patterns shown in Fig. 1, where we show the time evolution of space averaged values of the model variables, with $\tau = 4$, when uniform (ODE) and non-uniform initial conditions are considered. The time evolution pattern is characterized by a primary infection (time scale $\sim$ a few weeks), followed by a latency phase [1, 29] with a much larger time scale ($\sim$ years). After such phase, the number of healthy cells decay to much smaller values, what is interpreted as the AIDS phase, since the low immunity opens the door for opportunistic infections. The results for the ODE indicate that, for a specific set of parameter values the model is able to produce a time evolution pattern comprising three different phases: the primary infection, a long time-scale latency phase, and the final stage that can be associated with the AIDS onset. Irrespective of the other parameter values, all variables rapidly decay towards FP_1 when we set $\tau = 0$. In such case, the main features displayed in Fig. 1 disappear: the long latency phase vanishes and a direct switch from the primary infection to the AIDS phase occurs within a few weeks.

The ODE results in Fig. 1 were obtained for $A_0 = 0.05$.

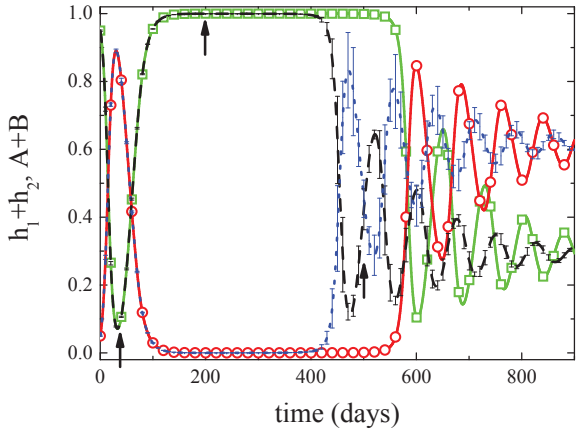

FIG. 1: Time evolution of healthy and infected $CD4^+T$ cells predicted by model (1). For uniform initial conditions, which correspond to the solution of an ODE system, squares and circles represent, respectively, H_1+H_2 and $A+B$ cell types. For non-uniform case, space average values for H_1+H_2 and $A+B$ cells are indicated by dashed and dotted lines, while error bars indicate the variance. Used parameter values, that satisfy the bounds discussed in Section II, are: k_1=0.163, k_2=0.228, k_3=0.650, k_4=3.25×10^{-5}, k_5=0.650, k_6=0.169, n=4, p=1, q=1.15. For the ODE solution, $H_{1,0}$=0.95, A_0=0.05. For the non-uniform conditions, $A_0 = 0.05$ except for a small square ate the center of the lattice where it assumes the value $A_0 = 0.06$.

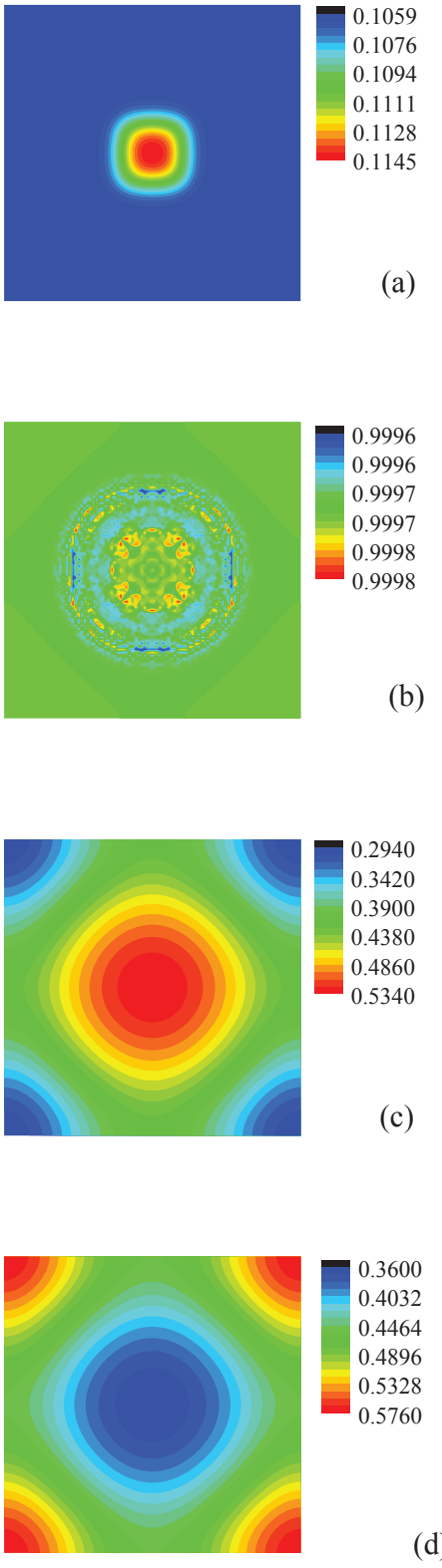

FIG. 2: Panels (a), (b) and (c) show three spacial patterns for the fraction of healthy cell population $H_{1,0} + H_{2,0}$ at $t_1 = 40, t_2 = 200$ and $t_3 = 500$ days formed on a patch of thyme tissue. The inhomogeneous initial conditions consist of larger amount of infected cells in the center of a square lattice. The dynamic evolution depends on the value of the diffusion coefficient k_9 (here 2×10^{-4}). Independent color codes are used for each panel. Despite the fact that fluctuations almost disappear during latency phase, they are able to increase largely during the approach to the HIV phase. In panel (d) we illustrate, for $t = t_3$, that the pattern for the infected cell population $(A+B)$ is highly anti-correlated with that for the healthy one $(H_{1,0} + H_{2,0})$.

The resulting trajectories have a smaller latency if the initial virus load is increased while, if A_0 decreases, the latency increases and the solution eventually reaches the situation of permanent cure. The effect of a very simple non uniform initial conditions is also displayed in Fig. 1. There we show the effect of starting with the larger value $A_0 = 0.06$ at the a small square in the center of the sample. Although this is an unrealistic conditions, it helps us to understand how the disease spreading depends on non-uniform conditions. The resulting effect is to reduce the latency phase with respect that we obtained for the ODE with $A_0 = 0.05$. The same effect is obtained if the rest of the cells outside small square is such as to lead to a permanent cure. This result indicates that the coupling mediated by k_9 is able to contaminate the whole thyme tissue. We postpone to the next paragraphs the influence of the k_9 value on the pattern formation.

In Fig. 2 we show three snapshots of spatial patterns corresponding to the sum $H_{1,0}+H_{2,0}$ for $t_1 = 40, t_2 = 200$ and $t_3 = 500$ days, as indicated by arrows in Fig. 1. The last panel draws the space dependence of $A + B$ for $t_3 = 500$. The results illustrate how the more rapid dynamics in the central area spreads over the whole tissue. Note that different color codes are used in each panel. During the latency phase the differences in cell population are minute across the tissue. After this phase, the limits of the color codes are far apart, an effect that is also reflected in the size of the error bars in Fig. 1. However, as the solution becomes globally attracted to the FP_1, differences in cell population are reduced again as $t \to \infty$. Finally, panel (d) illustrates that $H_1 + H_2$ and $A + B$ are strongly anti-correlated and complementary so that, for the majority of for all purposes, it is sufficient to draw just one of the graphs.

Once we have illustrated the kind of possible effect resulting from a particularly ordered inhomogeneous initial conditions, we consider now $H_{1,0}(\overrightarrow{r}) = \langle H_{1,0}(\overrightarrow{r})\rangle + \alpha\eta(\overrightarrow{r})$, where $\eta(\overrightarrow{r})$ represents a random number in the interval $[-1, 1]$ and α is the amplitude of fluctuations around the averages values $\langle H_{1,0}\rangle$. In such random configurations, we consider $A_0(\overrightarrow{r}) = 1 - H_{1,0}(\overrightarrow{r})$, so that $\langle H_{1,0}\rangle + \langle A_0\rangle = 1$. Let us briefly mention that another possible choice of initial conditions is to choose values of $H_{1,0}(\overrightarrow{r})$ to be only 0 or 1, with prescribed probabilities such that the pre-selected values for $\langle H_{1,0}\rangle$ and $\langle A_0\rangle$ are obtained. This procedure, however, is more suitable to be used when working with discrete valued variables, as in the CA model [17]. In the adopted choice, the initial virus load in different patches of thyme tissue is the coarse grained equivalent to a random assignment of infectious cells in the CA description.

The random choice of initial conditions makes it more evident that the different time scales in the three phase time evolution influence, in largely distinct ways, the spatial pattern formation. In other words, the relative magnitude of k_9 with respect to the other time scales present in the model plays a crucial role in the propagation of non-uniformities on the thyme tissue. Depending on this

value, a non-uniform initial state can lead to a homogeneous HIV distribution in any of the quoted phases, i.e., already in the primary infection, during the latency phase, or only after AIDS onset. For a typical three-phase evolution pattern shown in Fig. 1, we have noticed that the longest and largest influence occurs when $k_9 < 10^{-3}$. For values of k_9 of this order of magnitude or larger, the Laplacian terms contribute to a very rapid reduction of the difference in HIV infected cells between the neighboring patches of the thyme tissue. This can be illustrated by the pattern snapshots in Fig. 3 and time evolution curves in Fig. 4, for the same parameter values used in Fig. 1, while initial conditions are based on $\langle H_{1,0}\rangle = 0.95$ and $\alpha = 0.03$.

In the former one, we show snap-shots of $H_1 + H_2$ for different values of time, when $k_9 = 2 \times 10^{-4}$. The panels at $t_1 = 10, t_2 = 100$, $t_3 = 400$ and $t_4 = 600$ days were selected in such a way as to illustrate the spatial pattern in the different phases of the infection course. It is important to observe that each panel has color codes of its own, which is affected also by the amplitude range Δ.

The first panel, when $t_1 = 10$ corresponds to the primary infection, still suffers the influence of the random initial conditions. The amplitude of fluctuations is larger than that at $t = 0$ and this will prevail until the short before $t_2 = 100$, when system is about to move into the second phase (latency). The pattern is much more uniform than that at $t_1 = 10$, although no clear target can be identified. The fluctuations measured by Δ are minute, due to the fact that the system is globally attracted to the region of very slow dynamics close to $\widehat{FP0}$. The panel at $t_3 = 400$ illustrates the behavior after the system enters the third phase of the infection. Two targets in phase opposition are clearly recognizable. They surely have evolved from the still unformed intermediate pattern at t_2 and the fluctuations are very large. The same spatial modulation will be present for all values of t, as illustrated at $t_4 = 600$ in panel (d). The fluctuations are smaller than in the previous panel, a tendency that is observed if larger values of t are considered. Indeed, as $FP1$ is the globally attracting set, it turns out that Δ decays to 0 as $t \to \infty$. The panels suggest that the system evolves from random initial conditions towards a robust stationary wave pattern, the modulation of which is strongly dependent of the phase in which the system is found.

Let us now discuss the time evolution of the space averaged values of the variables shown in Fig. 4. There we recognize several characteristic features of the uniform time evolution patterns exhibited in Fig. 1. The spatial dispersion of the variables (σ), indicated by error bars, are directly related to the range of variation Δ of the color codes used in Fig. 3. We notice that they are strongly reduced whenever the system transits through a a close neighborhood of the FP's in phase space.

In Fig. 4 we can also appreciate the influence of k_9 on the solutions of system (1), keeping fixed the same

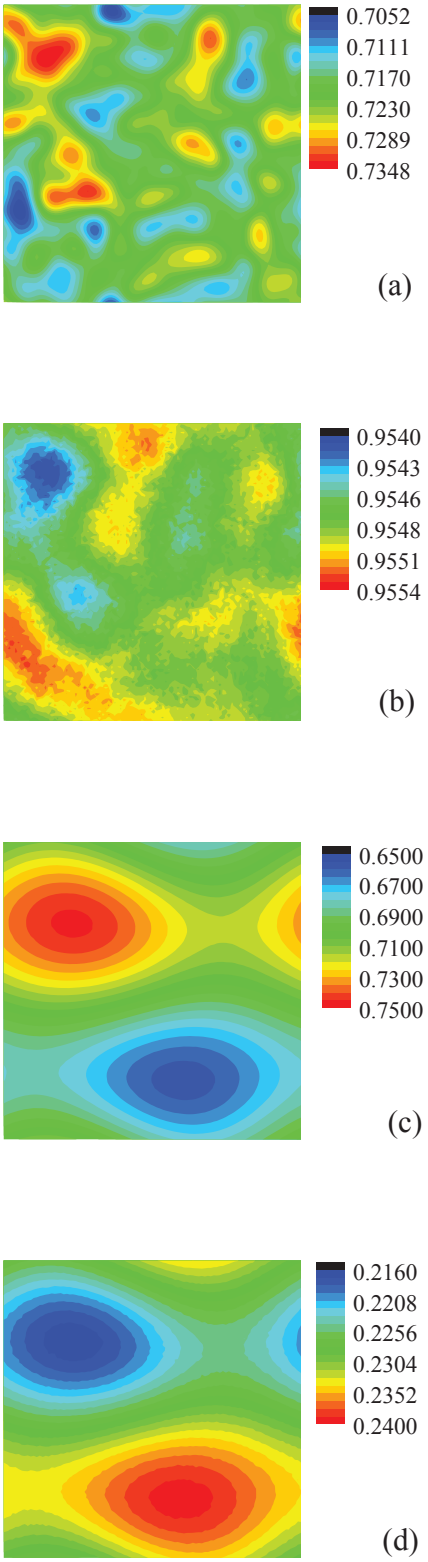

FIG. 3: Four spacial patterns for the fraction of healthy cell population $H_{1,0} + H_{2,0}$ at $t_1 = 10$ (a), $t_2 = 100$ (b), $t_3 = 400$ (c) and $t_4 = 600$ days (d) resulting from random inhomogeneous initial conditions, for the same parameter values used in Fig.2, $\langle H_{1,0}\rangle = 0.95$ and $\alpha = 0.03$. At early stages, the pattern reflects the initial randomness. Such influence lasts until the beginning of latency phase. During its long duration, fluctuations are minute as in Fig. 2. Despite this, a small number of large coherent patches, with much larger amplitudes and out of phase, develop in the third phase where AIDS sets in.

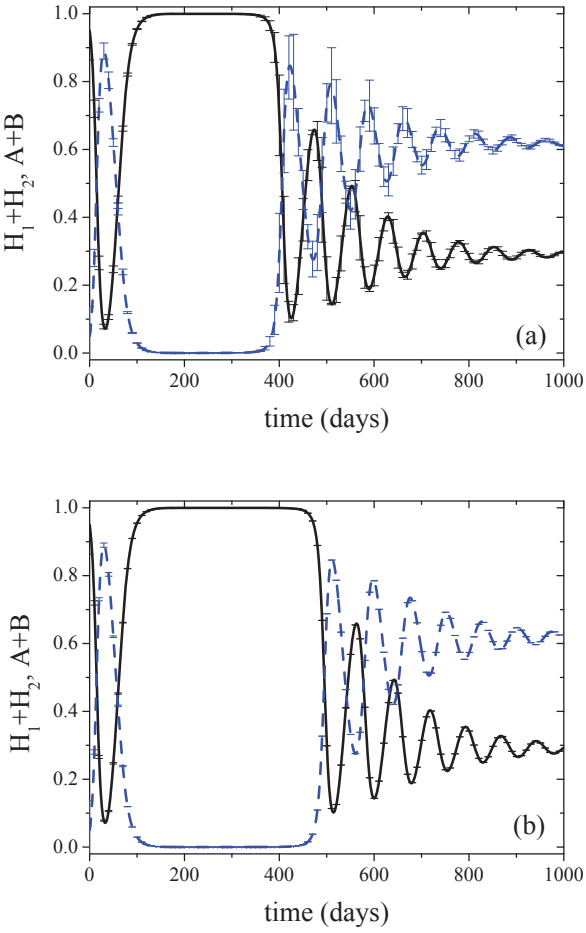

FIG. 4: Time evolution of fluctuation amplitudes σ for different values of $k_9 = 2 \times 10^{-4}$ (a) and 2×10^{-3} (b). Solid and dashed lines indicate $H_{1,0} + H_{2,0}$ and $A + B$, respectively. For the sake of a better visualization, the error bars (value of σ) have been amplified by a factor 5. Minute fluctuations during the latency phase do not avoid the development large fluctuations when k_9 is small. In (b), the large value of k_9 avoids the development of any appreciable fluctuation.

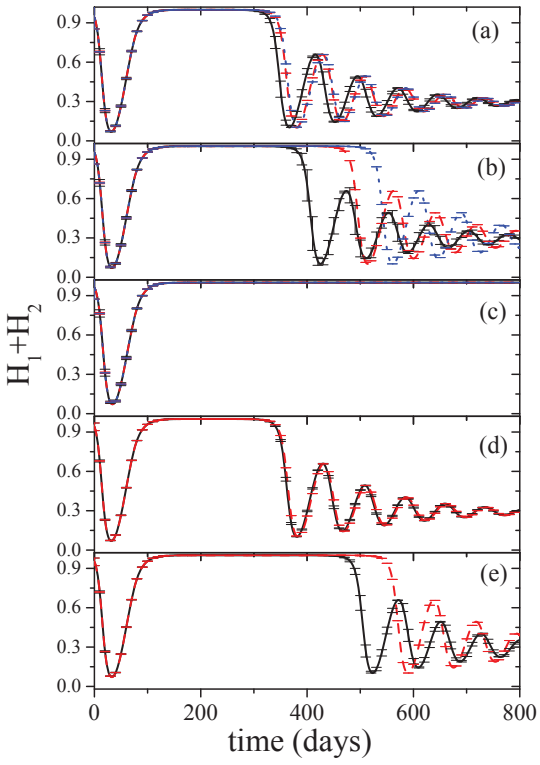

FIG. 5: Dependence of fluctuation size and latency duration on k_9, $\langle H_{1,0} \rangle$ and α. In Figs. 5(a)-5(c), solid line, dashes and dots correspond to $k_9 = 2 \times 10^{-4}, 2 \times 10^{-3}$ and 8×10^{-3}. The displayed curves, obtained when $\alpha = 0.03$, show that the latency increase with $\langle H_{1,0} \rangle$. When $\langle H_{1,0} \rangle = 0.95$, The influence of k_9 on latency size is enhanced. Otherwise, k_9 influences overall the fluctuation amplitudes. In Figs. 5(d)-5(e), when $\alpha = 0.01$, solid line and dashes correspond to $k_9 = 2 \times 10^{-4}$ and 2×10^{-3}. Fluctuations are reduced with respect to Figs. 5a-c. Latency size are almost insensitive to changes in α when $\langle H_{1,0} \rangle = 0.94$. However, when $\langle H_{1,0} \rangle = 0.95$, latency increases if α is reduced.

set of parameters used in the previous figures. The results for $k_9 = 2 \times 10^{-3}$ (Fig. 4(b)) indicate that the range of variation in the primary infection are considerably smaller than those for $k_9 = 2 \times 10^{-4}$ (Fig. 4(a)). As for the previous value of k_9, the error bars in Fig.4 show that the fluctuations are much larger during the primary infection than during the latency phase, when they becomes minute. However, a major difference to the previous values of k_9 is that error bars remain very small during the whole phase of AIDS onset. This indicates that, for practical purposes, the infected $CD4^+T$ population is uniformly distributed over the thyme tissue. The same situation is observed for still larger values of k_9.

Regarding the temporal evolution of average values, the results in Figs. 4(a) and 4(b) also illustrate that the value of k_9 influences the duration of the latency phase in a quite complex way. The latency duration is reduced when k_9 is small, but it grows and becomes fairly constant when this parameter increases. The reason for such behavior is that, due to small coupling among the thyme patches, cells enter the latency phase with distinct virus load. Those with a slightly larger amount of virus (A and B cells) will leave the neighborhood of $\widehat{FP0}$ at earlier time. This triggers the increase of infection of the neighboring patches and reduces the latency phase. For larger values of k_9, the more infected cells that could trigger the early leave of the latency phase have had their virus load distributed over the whole tissue. They become much strongly bounded to the majority of cells that are able to resist to the attraction of $FP1$.

Besides the displayed dependence on the value of k_9, the fluctuations and the duration of latency phase are influenced by the initial virus load $\langle H_{1,0}\rangle$ and initial randomness α. In Fig. 5, we show, for $H_1 + H_2$ only, results obtained when $H_{1,0} = 0.94, 0.95$ and 0.96 (for the same value $\alpha = 0.03$), as well as when $H_{1,0} = 0.94$ and 0.95 for $\alpha = 0.01$. The reduction of latency phase for smaller values of $\langle H_{1,0}\rangle = 0.94$ is in accordance with the ODE solution when the same parameter values are considered. The value of k_9 continues influencing the side of fluctuations in the third phase, but has much less effect on the latency duration as compared when $\langle H_{1,0}\rangle = 0.95$. The infinite latency phase, equivalent to complete healing, observed when $\langle H_{1,0}\rangle = 0.96$ also agrees with the ODE result. It is important to observe that fluctuations in the local initial values of $H_{1,0}$ are not sufficient to deviate the global behavior from being attracted to $\widehat{FP0}$. The influence of the value α becomes more evident when $\langle H_{1,0}\rangle = 0.95$. In such case, the latency phase becomes larger than those for larger values of α and corresponding values of k_9. We can observe that, despite smaller values of fluctuations during the primary infection and latency phase, these may still become much larger in the third phase when k_9 is small. The reasons for this dependence is the same as discussed above. For $\langle H_{1,0}\rangle = 0.94$ and 0.95 (not shown), the latency duration is much like those observed when $\alpha = 0.03$.

IV. CONCLUSIONS

This study considers a PDE system with time delay to describe the evolution of $CD4^+T$ cells on a thyme tissue under the attack of HIV population. It is based on the basic assumptions that important steps of HIV infection is localized on the thyme tissue and uses the same set of elementary contact steps among healthy and infected $CD4^+T$ cell that were able to provide the evolution in CA and ODE models. In order to emphasize the dependence of our results on the diffusion coefficient k_9 and initial conditions ($\langle H_{1,0}\rangle$ and α), we presented results for very specific values of the other parameters already present in ODE version of the model. Indeed, with such choice, the effect of the new ingredients of the model on latency duration and fluctuation size are enhanced and can be better appreciated by the reader.

The main results reported in this work refer to the identification of the influence of non-linear diffusion terms to describe the spread of infected cells over the healthy tissue. We have identified that, depending on the value of diffusion coefficient, homogeneous or standing wave patterns can be present. This dependence may be traced back to the interplay of different time scales present in the original ODE model. A very large diffusion coefficient promotes a very effective homogeneity in the tissue patches prior to the start of the latency phase, where fluctuations become smeared off. On the other extreme, small diffusion coefficients cause fluctuations in cell population, although minute, to remain present during the log latency phase, so that space dependent patterns will be present during the whole course of the infection. The interplay of different time scales, initial fluctuation size and magnitude of diffusion coefficient influences the fluctuation size and the duration of latency phase in a rather complex way. Finally, we would like to stress that, due to the intrinsic difficulties to combine space dependence with time delay effect, this work may provide valuable insights to the study of similar models with the same kind of complex structure. Indeed, a major part of the efforts required to find the solutions we reported herein was devoted to write and validate a stable numerical code for the integration of system (1).

Acknowledgements: This work was partially supported by the following Brazilian funding agencies: CAPES, FAPESB/PRONEX, CNPq and National Institute for Science and Technology/Complex Systems.

V. APPENDIX - LINEAR STABILITY ANALYSIS OF FP_1

The stability analysis can be performed for $\tau = 0$ and $\tau > 0$. The characteristic equation $M(\lambda) = det(J - \lambda I) = 0$ for the eigenvalues of the Jacobian stability matrices J defined in a neighborhood of PF_1 is obtained in a straightforward way. However, if $\tau > 0$, $det(J - \lambda I) = 0$ becomes a transcendental equation, with terms $\sim \exp -\lambda\tau$.

When $\tau = 0$, we obtain analytical, yet complicated, polynomial equation for the eigenvalues. J always has an identically vanishing eigenvalue (λ_0), which is associated to the conservation law in the number of cells. So, in principle, it is possible to obtain analytic expressions for all eigenvalues, provided the analytical expressions for FP_1 could be found. The analytical expressions are so complicated that it is better to find the eigenvalues by numerical means. Even with this restriction we can obtain important quantitative as qualitative insights on the stability properties.

The spectral properties of the system are robust, i.e., almost any choice of the parameters is representative of most of the other situations. Consider what happens to the model when the parameter values are set to $k_1 = 0.054$, $k_2 = 0.0675$, $k_3 = 0.20626500$, $k_4 = 0.00001$, $k_5 = 0.143$, $k_6 = 0.01$, $p = 1$, $q = 1.13$, $n = 4$. For these values, $FP_1 = (0, 0.377306, 0.302017, 0.241613, 0.0790638)$. Besides $\lambda_0 = 0$, we identify $\lambda_1 = -0.21216$, a coupled of complex conjugate eigenvalues $\lambda_{2,3}$ such that $Re\lambda_{2,3} = -0.04432$ and $\lambda_4 = -0.03832$. The eigenvalue λ_1 determines a rapid decay dynamics to a two-dimensional space, where a slow decay to FP_1 described by $\lambda_{2,3}$ takes place. So, FP_1 is a stable focus. This pattern does not change for the region of interest to model actual HIV infections.

If $\tau = 4 > 0$, it is not possible to make definite statements about the number of eigenvalues and we must re-

sort to other strategics to identify them. We used a standard iterative Newton-Raphson (NR) procedure to look for real and complex eigenvalues. We failed to detect any new real eigenvalue other than λ_1 and λ_4. The new values have only slightly changed with respect to those at $\tau = 0$. Regarding complex eigenvalues, it is possible to find a large number of them, all of which are characterized by a negative real part. Thus, all numerical evidences we obtain indicate that $\tau > 0$ does not change the attracting character of the stable focus.

A very important quantitative result follows from the numerical search for eigenvalues. Let us call $\lambda_{2,3}$ that pair of complex eigenvalues for which the absolute value of their real part is the smallest one. They are relevant as they dictate the pace at which a trajectory is attracted to the stable focus. We find out that, for the same parameter values, $Re(\lambda_{2,3}) = -0.002478$. Since this value is less than 1/10 of that found when $\tau = 0$, the stability analysis indicates that time delay causes a much slower decay dynamics in the neighborhood of FP_1. This means that the onset of AIDS after the latency phase is much slower than when compared with that with $\tau = 0$.

For more details and illustration please see reference [19].

[1] A. S. Perelson and P. W. Nelson, SIAM Rev. **41**, 3 (1999).
[2] M. J. P. A. Nelson, P.W., Math. Biosci. **163**, 201 (2000).
[3] M. Nowak and R. May, *Virus dynamics: Mathematical principles of immunology and virology* (Oxford University Press, Oxford, 2000).
[4] M. Stafford, L. Corey, Y. Cao, E. Daar, D. Ho, and A. Perelson, J. Theor. Biol. **203**, 285 (2000).
[5] R. Culshaw and S. Ruan, Math. Biosci. **165**, 27 (2000).
[6] R. Mannion, H. Ruskin, and R. Pandey, Theory in Biosciences **119**, 10 (2000), ISSN 1431-7613.
[7] R. Mannion, H. Ruskin, and R. Pandey, Theory in Biosciences **119**, 145 (2000), ISSN 1431-7613.
[8] P. W. Nelson and A. S. Perelson, Mathematical Biosciences **179**, 73 (2002), ISSN 0025-5564.
[9] M. Di Mascio, R. Ribeiro, M. Markowitz, D. Ho, and A. Perelson, Math. Biosci. **188**, 47 (2004).
[10] A. Landi, A. Mazzoldi, C. Andreoni, M. Bianchi, A. Cavallini, M. Laurino, L. Ricotti, R. Iuliano, B. Matteoli, and L. Ceccherini-Nelli, Computer Methods and Programs in Biomedicine **89**, 162 (2008).
[11] M. Barão and J. Lemos, Biomedical Signal Processing and Control **2**, 248 (2007).
[12] X. Zhou, X. Song, and X. Shi, Journal of Mathematical Analysis and Applications **342**, 1342 (2008).
[13] L. Cuifang and Y. Zhaohui, Journal of Mathematical Analysis and Applications **352**, 672 (2009).
[14] R. Culshaw, S. Ruan, and G. Webb, J. Math. Biol. **46**, 425 (2003).
[15] R. M. Jafelice, B. Bechara, L. Barros, R. Bassanezi, and F. Gomide, Mathematical and Computer Modelling **50**, 32 (2009).
[16] O. Cohen, G. Pantaleo, G. Lam, and A. Fauci, Springer Semin Immunopathol. **18**, 305 (1997).
[17] R. M. Zorzenon dos Santos and S. Coutinho, Phys. Rev. Lett. **87**, 168102 (2001).
[18] G. Solovey, F. Peruani, S. P. Dawson, and R. M. Z. dos Santos, Physica A **343**, 543 (2004).
[19] F. S. Bacelar, R. F. S. Andrade, and R. M. Z. dos Santos, arXiv:1003.5992v2 [physics.bio-ph] 1 Apr 2010 (2010).
[20] Y. Kuang, *Delay Differential Equations with Applications in Popopulation Dynamics* (Academic Press, Boston, 1993).
[21] L. Berezansky, E. Braverman, and A. Domoshnitsky, Differential Equations and Dynamical Systems **16**, 3 (2008).
[22] L. Berezansky, L. Idels, and L. Troib, Nonlinear Analysis Series B: Real World Applications **12**, 436 (2011).
[23] G. Pantaleo, C. Graziosi, and A. S. Fauci, N. Engl. J. Med. **328**, 327 (1993).
[24] D. P. Campos, S. R. Ribeiro, B. Grinsztejn, V. G. Veloso, J. G. Valente, F. I. Bastos, M. G. Morgado, and A. J. Gadelha, AIDS **19**, S22 (2005).
[25] A. Koch and H. Meinhardt, Review of Modern Physics **66**, 1481 (1998).
[26] P. Maini and H. Othmer, *Mathematical models for biological pattern formation* (Springer Verlag, New York, 2001).
[27] R. A. Koup, J. T. Safrit, Y. Cao, C. A. Andrews, G. McLeod, W. Borkowsky, C. Farthing, and D. D. Ho, Journal of Virology pp. 4650–4655 (1994).
[28] P. AN., Science **271**, 497 (1996).
[29] P. J. Delves, S. J. Martin, D. R. Burton, and I. M. Roitt, *Roitt's Essential Immunology* (Wiley-Blackwell, 2011), 12th ed.

***Submission Checklist - "Confidential information for the Editor"**

Dear Editor,

all files have been included in th on-line submission:

1 tex file for the manuscript
1 bib file for the bibliography
2 intermediary files: one pdf file with authors generated manuscript and one bbl file generated from the bib and tex files
12 figure files